Carrier capture in InGaN/GaN quantum wells: Role of electron-electron scattering

Carrier capture in InGaN/GaN quantum wells: Role of electron-electron scattering

Marco Vallone, Michele Goano, Francesco Bertazzi, and Giovanni Ghione

Citation: Journal of Applied Physics **121**, 123107 (2017); doi: 10.1063/1.4979010
View online: http://dx.doi.org/10.1063/1.4979010
View Table of Contents: http://aip.scitation.org/toc/jap/121/12
Published by the American Institute of Physics

Carrier capture in InGaN/GaN quantum wells: Role of electron-electron scattering

Marco Vallone,[1,a)] Michele Goano,[1,2] Francesco Bertazzi,[1,2] and Giovanni Ghione[1]
[1]*Dipartimento di Elettronica e Telecomunicazioni, Politecnico di Torino, corso Duca degli Abruzzi 24, 10129 Torino, Italy*
[2]*IEIIT-CNR, Politecnico di Torino, corso Duca degli Abruzzi 24, 10129 Torino, Italy*

(Received 19 October 2016; accepted 9 March 2017; published online 27 March 2017)

The competition of electron-electron interband scattering (*ee*) and longitudinal optical phonon emission (*e-ph*) as electron capture mechanisms is theoretically investigated in III-nitride quantum wells. The non-trivial separation of their scattering probabilities is discussed, and compact expressions for capture time are obtained in the framework of the quantum many-body formalism. At the typical operating conditions of light emitting diodes (LEDs), the model predicts an increasing importance of *ee* scattering as a capture mechanism with increasing carrier density. Verifications against recent experiments are presented to support this finding and confirm the need for population-dependent capture time expressions including both *ee* and *e-ph* mechanisms for an accurate description of LED carrier dynamics and efficiency. *Published by AIP Publishing.*
[http://dx.doi.org/10.1063/1.4979010]

I. INTRODUCTION

Intense investigations are currently ongoing about the nature of the internal quantum efficiency (IQE) droop in GaN-based light-emitting diodes (LEDs) at high current and temperature.[1–5] Numerical simulations of quantum well (QW) LEDs are largely based on drift-diffusion simulators, whose inadequacies related to several nitride-specific issues have been generally addressed with *ad hoc* models (e.g., for ballistic overshoot, carrier overflow, tunneling assisted by phonons, and crystal defects), often based on poorly known or ill-defined physical parameters.[6–8]

In semiclassical models of LED transport dynamics, the carrier capture and escape times between bulk unbound states and QW bound states are among the most critical quantities for a correct estimate of the IQE droop.[5,9] In spite of their importance, capture/escape times are usually treated as fitting parameters, and their dependence on the excitation conditions is customarily neglected.

Electron capture in QWs may take place through electron-electron (*ee*) scattering, relaxation on defects, longitudinal optical (LO) phonon emission (*e-ph*), multi-phonon emission, tunneling, etc. (see, e.g., Refs. 10 and 11 and references therein). Among these processes, capture via LO-phonon emission τ_{e-ph}, besides concurring to the determination of the total QW capture time to a considerable extent,[11–13] is interesting because it is determined by the LO-phonon-electron self-energy Σ^{e-ph}, a quantity that also affects the phonon-assisted Auger recombination lifetime.[14–18] At high carrier densities, capture via *ee* scattering may also become very effective, and the relative importance of *ee* and *e-ph* mechanisms should be assessed. (In the present work, only electrons will be considered, but the formalism also applies to hole capture.)

In a previous work,[19] we presented a quantum model which is able to reproduce the experimental capture time in InGaN/GaN QWs as a function of bulk and QW carrier densities N and N_{QW}, considering, however, only the *e-ph* process, without addressing *ee* scattering. The importance of the latter as a capture mechanism in III-nitride QWs is controversial: ultrafast pump-probe experiments[12,20–23] indicate a probable contribution from both mechanisms, in one case[12] reporting also numerical estimates of the *overall* capture time τ as a function of N. In recent experiments, David *et al.*[9] obtained indications of a τ with two components, one compatible with LO-phonon emission and a second one possibly related to *ee* scattering. For the III-nitride materials system, no theoretical, first-principles works allow to clearly distinguish among individual contributions to the overall capture rate. In conventional III-V-based QWs, the relative importance of *ee* and *e-ph* scattering rates was calculated in Ref. 24 for AlGaAs/GaAs QWs within the static screening and second-order Born approximations, and *ee* scattering was found to be quite effective. Also, employing simple static screening, the two capture mechanisms were found to be of comparable magnitude in Ref. 10, at least for high carrier densities. Valuable theoretical calculations[25–27] employing frequency dependent screening in the Random Phase Approximation (RPA) formalism[28,29] revealed a significant decrease in the capture time with N; however, these fully numerical approaches do not lead to formulations ready to be employed in device-level simulators.

In Sec. II, following the quantum many-body formalism and employing the RPA dielectric function in the dynamical form (frequency and momentum dependent) of the Single Plasmon Pole (SPP) approximation,[28–30] we present explicit, analytic expressions of capture time for the *ee* scattering mechanism, as functions of carrier density and InGaN/GaN QW parameters. Electron eigenfunctions are evaluated here within the flat band and effective mass approximations, with

[a)]Electronic mail: marco.vallone@polito.it

parameters according to Ref. 31, but the proposed approach can be applied with no modifications also when potential and carrier density profiles are determined by solving the Poisson and Schrödinger equations selfconsistently,[32] also taking into account the interface polarization charges.[11,33] The results obtained with the present method are compared in Sec. III with the experimental data from Ref. 9 (for *ee* scattering) and from Ref. 12 (for *e-ph* and *ee* processes).

II. THEORY

The *e-ph* and the *ee* elementary interactions are described, respectively, by the unscreened Frölich and Coulomb potentials $V_{\rm ph}$ and $V_{\rm ee}^{\infty}$.[29] At the lowest perturbative order, two electrons can interact exchanging a *virtual* LO-phonon or photon, as shown in Fig. 1(a). At higher perturbative orders, the two considered scattering processes become deeply connected, as shown, e.g., by the 2nd order diagrams in Fig. 1(b). At each perturbative order, several diagrams contain both *ee* and *e-ph* elementary interactions, represented in the figure by a wavy or dashed line, respectively, and in the transition amplitude by a factor $V_{\rm ee}^{\infty}$ or $V_{\rm ph}$, according to the Feynman's rules.[29,30] Their expressions $V_{\rm ee}^{\infty} = V_{\rm ee}/\epsilon_{\infty} = 4\pi e^2/(\epsilon_0\epsilon_{\infty}|\boldsymbol{q}|^2)$ and $V_{\rm ph} = -M_{|\boldsymbol{q}|}^2 D_0(\omega_m)$ are presented and discussed in Ref. 29: $M_{|\boldsymbol{q}|}^2 = (1/2)K_{\epsilon}\omega_{LO}V_{\rm ee}$ is the square of the unscreened electron-phonon matrix element, $K_{\epsilon} = \epsilon_{\infty}^{-1} - \epsilon_s^{-1}$, ϵ_{∞} and ϵ_s are the dynamic and static dielectric constants, $D_0(\omega_m) = 2\omega_{LO}/(\omega_m^2 - \omega_{\rm LO}^2)$ is the unscreened phonon propagator,[19,29] ω_{LO} is the polar LO-phonon frequency, $\boldsymbol{q}$ is the *virtual* phonon or photon wavevector, ω_m its (bosonic) frequency, and ϵ_0 and e are the vacuum dielectric permittivity and the elementary charge. Thus, considering diagrams with a single polarization bubble, there are four possible diagrams (Fig. 1(b)), and diagrams with n bubbles have 2^{n+1} possible arrangements. The effective *ee* plus *e-ph* interaction $V_{\rm eff}$ in RPA can be found summing up to infinite perturbative order all possible n-bubble diagrams (Fig. 1(c)) according to Dyson's equation

$$V_{\rm eff} = (V_{\rm ee}^{\infty} + V_{\rm ph})/\left[1 - (V_{\rm ee}^{\infty} + V_{\rm ph})P\right],$$

where $P = (1-\epsilon)/V_{\rm ee}^{\infty}$ is the polarization of the electron gas and ϵ is the dielectric function. An important and non-trivial step is the separation of the effective *dressed* (dynamically screened) RPA interaction $V_{\rm eff}$ into its *ee* and *e-ph* contributions $V_{\rm ee,s}$ and $V_{\rm ph,s}$

$$V_{\rm ee,\,s} = \frac{V_{\rm ee}^{\infty}}{\epsilon}, \quad V_{\rm ph,\,s} = \frac{V_{\rm ph}}{\epsilon^2\left(1 - M_{|\boldsymbol{q}|}^2 D_0 P/\epsilon\right)}, \tag{1}$$

where the RPA-SPP dielectric function $\epsilon^{-1} = 1 + \Omega_{pl}^2/(\omega_m^2 - \omega_q^2)$ contains the N- and $|\boldsymbol{q}|$-dependent effective plasmon and plasma frequencies ω_q and Ω_{pl}.[29,34] Despite being formally distinct, a mutual interplay between the two screened Frölich and Coulomb interactions and related self-energies does exist at a very fundamental level: a detailed derivation of $V_{\rm ph,s}$ (see Ref. 29, Sec. VI C) shows that the obtained screened *e-ph* interaction includes the *ee* effects properly, and a straightforward derivation of the screened *e-ph* interaction from Dyson's equation without the Coulomb interaction would not include the extra factor $1/\epsilon$ in the $M_{|\boldsymbol{q}|}^2 D_0 P/\epsilon$ term contained in the expression of $V_{\rm ph,\,s}$ in Eq. (1).

A QW capture process via *ee* scattering consists of an electron belonging to a barrier state $\Psi_{\boldsymbol{k}_1}$ with energy E and wavevector $\boldsymbol{k}_1$ (the zero-point energy is the QW ground state) that interacts with a second electron with wavevector $\boldsymbol{k}_2$ ending in the nth QW state $\phi_{n,\boldsymbol{k}_1-\boldsymbol{q}}$, with the exchange of a virtual photon with wavevector $\boldsymbol{q}$ and frequency ω_m; the second electron can belong either to a barrier state $\Psi_{\boldsymbol{k}_2}$ or to the jth QW subband $\phi_{j,\boldsymbol{k}_2}$. Considering only the first case, the *ee* scattering RPA self-energy $\Sigma_{\boldsymbol{k}_1,\boldsymbol{k}_2}^{ee}(E)$ reads

$$\Sigma_{\boldsymbol{k}_1,\boldsymbol{k}_2}^{ee}(E) = \frac{-1}{\beta\hbar}\sum_{\boldsymbol{q},\boldsymbol{k}_2',\omega_m}\langle\Psi_{\boldsymbol{k}_2'}\phi_{n,\boldsymbol{k}_1-\boldsymbol{q}}|V_{\rm ee,s}|\Psi_{\boldsymbol{k}_1}\Psi_{\boldsymbol{k}_2}\rangle G_0. \tag{2}$$

Here, β is the inverse temperature in energy units, $G_0 = 1/[i\omega_m + i\omega - \hbar|\boldsymbol{k}_1 - \boldsymbol{q}|^2/(2m^*) - E_{\rm F}/\hbar]$ is Matsubara's single-particle propagator[19,28,29] where $\omega = E/\hbar$, $\hbar$ is the reduced

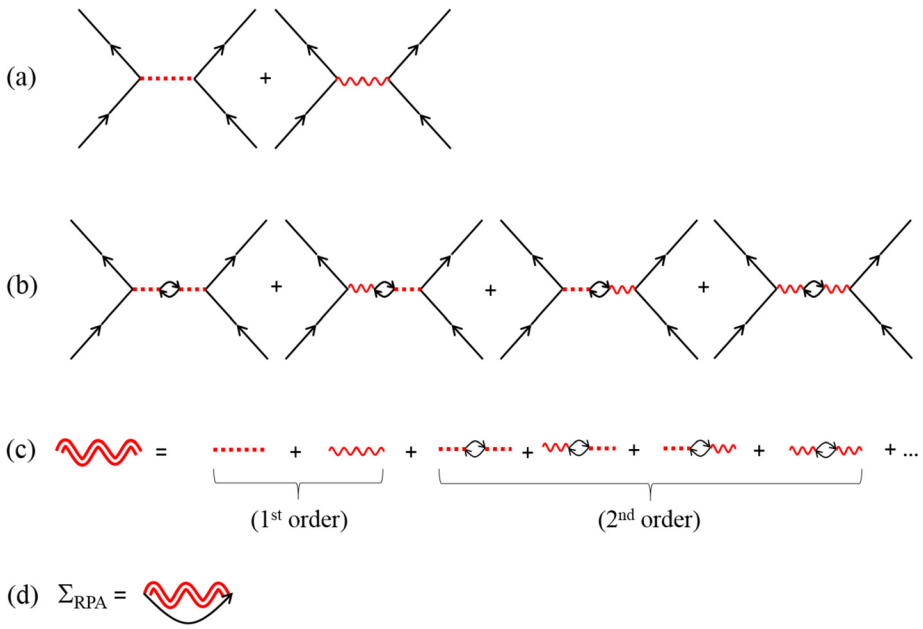

FIG. 1. (a) First order Feynman's diagrams for electron scattering exchanging a phonon (dashed line) or a photon (wavy line). (b) The four 2nd order Feynman's diagrams with one polarization bubble. Summing as geometrical series n-bubble contributions up to infinite order, the effective *dressed* RPA interaction (double wavy line) is obtained (c). The RPA self-energy (d), represented by a free particle propagator emitting and reabsorbing a quantum of dressed RPA interactions, contains both Frölich and Coulomb terms.

Planck's constant, m^* is the electron effective mass, and E_F is the Fermi energy.

$\Sigma^{ee}_{\boldsymbol{k}_1,\boldsymbol{k}_2}$ was evaluated with the following procedure:[19] (a) the $\boldsymbol{k}_2'$ summation was performed by exploiting a Dirac-δ factor stemming from the calculation of $\langle \Psi_{\boldsymbol{k}_2'} \phi_{n,\boldsymbol{k}_1-\boldsymbol{q}} | V_{\mathrm{ee,s}} | \Psi_{\boldsymbol{k}_1} \Psi_{\boldsymbol{k}_2} \rangle$, representing the momentum conservation at each vertex; (b) the summation over the frequency ω_m was done following the Matsubara formalism (the Fermi n_F and Bose n_B occupation factors appear during the summation thanks to the bosonic character of ω_m);[29] (c) the $\boldsymbol{q}$-summation was converted into an integral by exploiting the QW-plane translational invariance: considering for $\boldsymbol{q}$ and $\boldsymbol{k}_1$ their orthogonal and in-plane components $(q_z, \overrightarrow{q_\parallel})$ and $(k_{1,z}, \overrightarrow{k_{1\parallel}})$, the integration could be done analytically using residue theorems, after having extended the integration to a complex domain, first in q_z, then in $\overrightarrow{q_\parallel}$, without any truncation unlike in some numerical approaches.[25,26,35] In the end, we obtained

$$\Im\Sigma^{ee}_{\boldsymbol{k}_1,\boldsymbol{k}_2}(E) = \frac{\pi\alpha m^*\hbar c}{\epsilon_\infty}\int_0^{2\pi} d\theta\, I_{ee}(\theta)_{n,\boldsymbol{k}_1,\boldsymbol{k}_2} \times \frac{\Omega_{pl}^2}{\omega_q}\frac{(1+n_B-n_F)\Theta(E_{\mathrm{res}})}{\sqrt{2m^*E_{\mathrm{res}} - \hbar^2 k_1^2 \sin^2(\theta)}}, \quad (3)$$

where $\Im$ indicates the imaginary part, α is the fine structure constant, c is the light velocity, $k_{1,2} = |\overrightarrow{k_{1,2\parallel}}|$, $q = |\overrightarrow{q_\parallel}|$, θ is the angle between $\overrightarrow{q_\parallel}$ and $\overrightarrow{k_{1\parallel}}$, Θ is the Heaviside step function, $E_{\mathrm{res}} = E - E_F\,\Theta(E_F) - \hbar\omega_q$, and the form factor $I_{ee}(\theta)$ comes from the eigenfunctions overlap integral. The QW Fermi energy E_F (N_{QW}) was evaluated as a function of the equivalent two-dimensional (2D) QW carrier density, estimated as $N_{\mathrm{QW}}\,L_w$, where L_w is the QW width. All implicitly q-dependent quantities in Eq. (3), like, E_{res}, ω_q, or the Fermi distribution

$$n_F = \frac{1}{1+\exp\left[\beta\left(\frac{\hbar^2(k_1-q)^2}{2m^*} - E_F\right)\right]}, \quad (4)$$

for the QW states, were evaluated in the q-pole of the Green's function $q_p = k_1\cos(\theta) + \sqrt{2m^*E_{\mathrm{res}}(q_p)/\hbar^2 - k_1^2 sin^2(\theta)}$, expressing the momentum-energy conservation. Regarding n_B, in the present work, it was always set to zero for simplicity. The corresponding quantum capture time is defined as $1/\tau_{ee} = (2/\hbar)\Im\Sigma^{ee}/(1+n_B-n_F)$: since in rate equations it is customary to write the occupation factor $(1+n_B-n_F)$ explicitly, this position avoids to erroneously include it twice.

Regarding the capture process via phonon emission, it can be described as an electronic transition from an initial barrier state $\Psi_{\boldsymbol{k}_1}$ to a final QW state $\phi_{n,\boldsymbol{k}_1-\boldsymbol{q}}$ through the emission of a phonon of wavevector $\boldsymbol{q}$ and frequency ω_m. In RPA, the self-energy related to this process is

$$\Sigma^{e-ph}_{\boldsymbol{k}_1}(E) = \frac{-1}{\beta\hbar}\sum_{\boldsymbol{q},\omega_m}\langle\phi_{n,\boldsymbol{k}_1-\boldsymbol{q}}|V\mathrm{ph,s}|\Psi_{\boldsymbol{k}_1}\rangle G_0\,, \quad (5)$$

and following a procedure still based on complex integration and described in Ref. 19, we obtained

$$\Im\Sigma^{e-ph,\pm}_{\boldsymbol{k}_1}(E) = 2\pi K_\epsilon\omega_{LO}^2\alpha m^*\hbar c\int_0^{2\pi} d\theta\, I_{e-ph}(\theta)_{n,\boldsymbol{k}_1} \times F_\pm\frac{(1+n_B-n_F)\,\Theta\left(E^\pm_{\mathrm{res}}\right)}{\sqrt{2m^*E^\pm_{\mathrm{res}} - \hbar^2k_1^2\sin^2(\theta)}}, \quad (6)$$

where $E^\pm_{\mathrm{res}} = E - E_F\,\Theta(E_F) - \hbar\omega_\pm$, $I_{e-ph}(\theta)$ is a form factor ensuing from the wavefunction overlap integral, $F_\pm = (\omega_\pm^2 + \Omega_{pl}^2 - \omega_q^2)^2/[2\omega_\pm(\omega_\pm^2-\omega_q^2)(\omega_\pm^2-\omega_\mp^2)]$, and the upper or lower signs in $\Sigma^{e-ph,\pm}_{\boldsymbol{k}_1}$ refer to the emission of a phonon-plasmon mode of frequency $\omega_\pm$, where $\omega_\pm^2 = (\omega_q^2+\omega_{LO}^2)/2 \pm \sqrt{(\omega_q^2-\omega_{LO}^2)^2 + 4K_\epsilon\omega_{LO}^2\Omega_{pl}^2}/2$.

Since the two *e-ph* self-energies $\Sigma^{e-ph,\pm}_{\boldsymbol{k}_1}$ correspond to the emission of two possible and distinct LO-phonon-plasmons, two distinct quantum capture times $1/\tau^\pm_{e-ph} = (2/\hbar)\Im\Sigma^{e-ph,\pm}/(1+n_B-n_F)$ are possible. Therefore, the sum of RPA *ee* and *e-ph* self-energies represented in Fig. 1(d) provides the *overall* capture time $\tau = 1/(1/\tau_{ee} + 1/\tau^+_{e-ph} + 1/\tau^-_{e-ph})$ and depends on both N and N_{QW}.

The general procedure of frequency and momentum integration in the complex-plane in order to obtain self-energies is well known in the literature. Nevertheless, it is not customary in the derivation of capture times, and numerical approaches are usual when the dynamical RPA dielectric function, adopted in this work, is considered. However, an obvious drawback is the loss of the possibility to obtain simple, compact expressions, like Eq. (3) that we obtained following a long but straightforward procedure. Instead, considering the phonon emission, the method was already outlined by one of the authors in a previous work[36] and applied to III–V compounds. The formulation presented in Ref. 19 explained better several points, besides specializing the model to nitride-based QWs. In addition, it is worth emphasizing that the efforts in obtaining simple expressions like Eqs. (3) and (6) are rewarded by the possibility to achieve further simplified limiting forms (e.g., in low or high carrier density regimes, see an example in the discussion at the end of Section III), allowing to make comparisons and estimates in an easier way.

III. MODEL VALIDATION AND RESULTS

In order to validate the present model, we considered two sets of experimental data. The first (referred to as *set A* in the following) was obtained by Fan *et al.*[12] employing time-resolved differential transmission spectroscopy to evaluate the dependence of the *overall* capture time τ from N, for a nominally undoped 2.5 nm/7.5 nm $In_{0.08}Ga_{0.92}N$/GaN well-barrier system. The second (*set B* in the following) was recently presented by David *et al.*:[9] with a small-signal analysis of a 4 nm/30 nm $In_{0.09}Ga_{0.91}N$/GaN single QW-barrier heterostructure, the authors obtained indications of a τ with two components: a fast one, around 1 ps and attributed to the *e-ph* process, and a second one, proportional to $1/N$, much slower in the experimentally explored interval of N ($10^{12} < N < 10^{14}\,\mathrm{cm}^{-3}$), with a probable signature of *ee* scattering.

Adopting material parameter values reported in Refs. 19 and 31, we tested the present combined *ee* plus *e-ph* model against set A and set B data, separating the individual capture rate contributions and considering only the capture to the QW ground state.

A rate equation system like

$$\frac{dN}{dt} = \frac{I}{eV} - \frac{(1 + n_B - n_F)N}{\tau} + \frac{N_{QW}}{\tau_{esc}}, \tag{7a}$$

$$\frac{dN_{QW}}{dt} = -\frac{N_{QW}}{\tau_{rec}} - \frac{N_{QW}}{\tau_{esc}} + \frac{(1 + n_B - n_F)N}{\tau}, \tag{7b}$$

is able, in principle, to describe the time-evolution of the barrier and QW carrier density (the capture, escape, and recombination times are described, respectively, by τ, τ_{esc}, and τ_{rec}; I is the injection current and V the active region volume). Nevertheless, before proceeding, an important point to clarify is how to correctly manage the RPA approximation. In Ref. 37, chap. 14, an extensive discussion shows that the build up of the screening after a pulse excitation needs some time which is of the order of an inverse plasmon frequency in the system of excited carriers (a few femtoseconds).[38] As a consequence, the static approximation of the RPA is not suitable, and the dynamic RPA formulation (adopted in the present work, see Sec. I) is considered a better one. However, the solution of Eq. (7) in the time domain would lead to wrong results even in the latter case[37,38] since the RPA itself does not provide a rigorous description of the physics during a fast transient. A better approach is given, e.g., by the time-dependent Non-Equilibrium Green's Function (NEGF) formalism,[37–39] which is well beyond the scope of the present contribution, focused on obtaining expressions suitable for fast modeling tools, although approximate. Therefore, we adopted a different method.

Regarding set A (the pump-probe experiment), we calculated $\tau(N)$ without making use of Eq. (7) but instead considering the definition of τ, Eqs. (3) and (6), setting N_{QW} to a low value ($10^{13}\,cm^{-3}$, realistic during the very initial part of the transient), and varying N. This choice assumes the screening in barriers as already built-up, and the obtained $\tau(N)$ may be considered representative of the capture time experienced by electrons during the initial part of the transient.

By contrast, experimental data of set B refer to a voltage-driven single-QW LED, operated in the steady-state at current density regimes spanning from low to high injection. Therefore, in the study of set B, we self-consistently calculated $\tau(N, N_{QW})$ and N_{QW} itself as functions of N, ruled by Eq. (7), in which the time-derivatives were set to zero (steady-state). For this purpose, it can be noticed that only Eq. (7b) is needed, whereas Eq. (7a) may be eventually employed to connect carrier and current densities N and J.

Regarding the other lifetimes, in the present calculation, τ_{rec} was evaluated considering only radiative and Auger recombination processes as in Ref. 19 (remarks about the uncertainties and limitations of standard recombination models in nitrides can be found, e.g., in Refs. 6, 40, and 41). For τ_{esc}, we adopted a value of 3×10^{-10} s (see Ref. 9) able to reproduce the experimental data well. It has been observed that τ_{esc} not only strongly depends on L_w and T but is also affected by a possible background doping in the active region and by the bias current.[42] In addition, barrier tunneling competes with the thermionic escape with lifetimes around 0.1–1 ns,[42,43] besides other effects possibly at play, like tunneling assisted by defects.[5] As a consequence, in the present formulation, τ_{esc} should be regarded as a fitting parameter, more than a pure thermionic escape time, since it may include several not easily separable effects.

For both sets of experimental data, a fitting parameter $a \approx 0.13$ multiplies both overlap integrals I_{ee} and I_{e-ph}. This empirical factor scales the numerical values of the self-energies and is justified by the approximations considered for the wavefunctions and by our focus on estimating the relative importance of the involved processes rather than their absolute values.

Fig. 2 shows the calculated capture times for set A and set B for the three distinct processes:[44] *e-ph* via modes ω_- and ω_+ and *ee* scattering. Regarding set A (Fig. 2(a)), the differences between theoretical and experimental slopes may originate from the limited number of experimental points, covering a narrow range of N. The agreement between our theoretical τ_{ee} curve and the experimental data is much better for set B (Fig. 2(b)), probably also because the data span more than two decades in N, allowing to reduce the effects of local fluctuations.

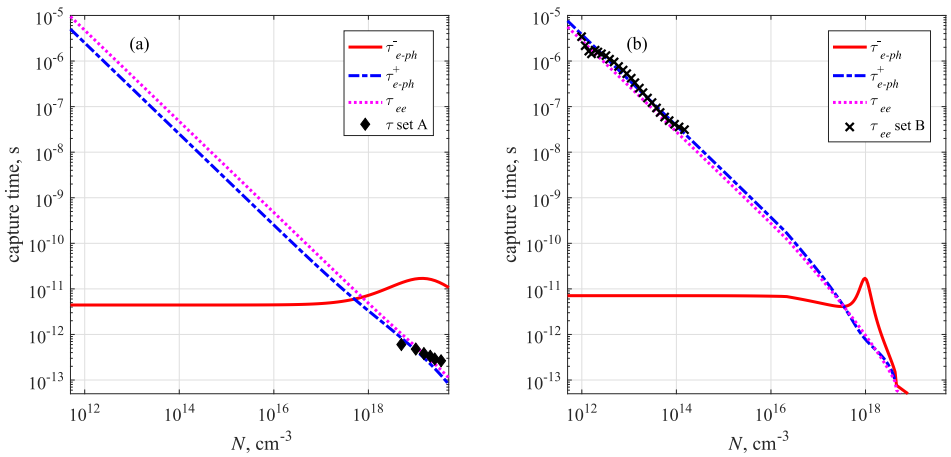

FIG. 2. Electron capture times $\tau^{\pm}_{e-ph}$ and τ_{ee}, calculated as functions of N, for set A (panel (a)) and set B (panel (b)). Experimental points are shown as symbols. The τ^{-}_{e-ph} peak at high carrier densities has been discussed in Ref. 19.

In Fig. 2, two intervals of N can be identified: in the low density regime, τ is mainly determined by LO-phonon emission as a ω_- phonon-plasmon mode, with characteristic time τ^-_{e-ph}. When the carrier density is increased, τ_{ee} and τ^+_{e-ph} progressively reduce, competing with τ^-_{e-ph} when N is above $\approx 10^{17}\,\mathrm{cm}^{-3}$. In the interval of N corresponding to set A experimental points (Fig. 2(a)) and also typical of LED operation, the capture time is mainly given by contributions coming from τ_{ee} and τ^+_{e-ph} at a similar extent, and therefore, investigations about the IQE droop in LEDs should exclude neither of these two mechanisms, and the customary approximation of the overall capture time τ with a constant value (see, e.g., Ref. 45) cannot be considered realistic. It may also be noticed that the dissimilarity between the two panels of Fig. 2 depends partly on the difference in the two active region thicknesses and partly on different ways we obtained the two results, as explained above.

Fig. 3 reports the carrier density N_{QW} versus N, calculated by Eq. (7b) in the steady-state for the parameters of set B, employing the present model for $\tau(N, N_{\mathrm{QW}})$ (solid line) and a fixed τ of $\approx$4 ps (dashed line). The difference between the two curves is not very large, but it suggests that the capture process is not inhibited by the potential screening, at least in stationary conditions: on the contrary, screening favors capture by increasing the energies $\hbar\omega_\pm$ and $\hbar\omega_q$, which get closer to $E - E_{\mathrm{F}}$ (resonance condition, see denominators in Eqs. (3) and (6)).

As a further consistency check, we calculated, employing set B parameters, the recombination time τ_{rec} and the injected current density J as functions of N, employing Eq. (7) in the steady-state, self-consistently evaluating τ and N_{QW}. Corresponding set B experimental points have been extracted from Fig. 3(a) of Ref. 9 at room temperature, and the comparison is shown in Fig. 4, where τ_{rec} is plotted vs. J, obtaining an overall satisfactory agreement.

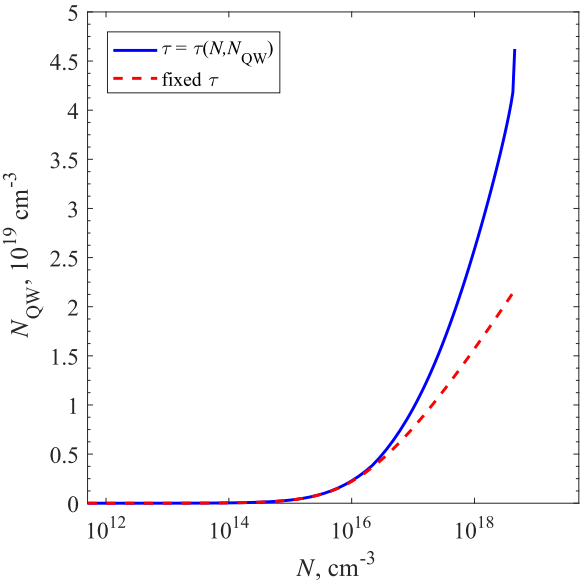

FIG. 3. Carrier density N_{QW} versus N calculated by Eq. (7b) in the steady-state for the parameters of set B, employing the present model for $\tau(N, N_{\mathrm{QW}})$ (solid line) and a fixed τ of $\approx$4 ps (dashed line).

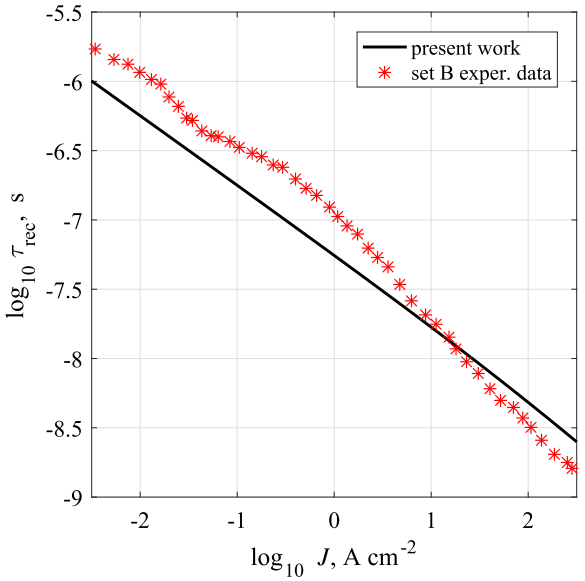

FIG. 4. Recombination time versus injected current density J, as obtained from the model (set B parameters), compared with the experimental data extracted from Fig. 3(a) of Ref. 9 at room temperature.

A few additional remarks are in order. First, when N decreases below $10^{16}\,\mathrm{cm}^{-3}$, we observed that $\omega_- \approx \omega_{LO}$ and $\omega_+ \approx \omega_q$. This means that ω_- is substantially a LO-phononic mode of frequency ω_{LO} unless N increases enough to screen the Frölich interaction and to couple phonon to plasmon, whereas ω_+ is substantially a plasmonic mode for all carrier densities. In addition, Ω_{pl} becomes progressively much smaller than the other frequencies, allowing to obtain the limiting forms $F_- \approx 1/2\omega_{LO}$ and $F_+ \approx \Omega^2_{pl}/(2K_\epsilon\omega_q\omega^2_{LO})$. Therefore, F_- becomes N-independent, justifying a similar behavior for τ^-_{e-ph}. Instead, F_+ tends to zero for decreasing N, making $\tau^+_{e-ph}(N)$ to loose importance when N reduces, with respect to the other two capture times. These two limiting forms of $F_\pm$ allow recovering known expressions of the capture time.[26]

Second, the closeness of $\tau_{ee}(N)$ and $\tau^+_{e-ph}(N)$ over several decades of N (in addition, they both scale as $1/N$) are worth of an explanation. Plasmons are collective excitations resulting from the quantization of carrier density oscillations, arising from a Hamiltonian for the long-range electron-electron correlations.[30] Intuitively, an electron can lose part of its energy exchanging a plasmon ω_+ only if the carrier density is not negligible, and the probability of this process is expected to increase with N. The same argument applies to the probability of the ee scattering; therefore, it is not unexpected that both processes exhibit the same trend with N. The argument is confirmed by the fact that, in the low-density regime, the limiting forms for self-energies become

$$\Im\Sigma^{e-ph,-} = \alpha\pi m^*\hbar c K_\epsilon \omega_{LO} \int_0^{2\pi} \frac{d\theta I_{e-ph}\,\Theta(E^-_{\mathrm{res}})}{\sqrt{2m^*E^-_{\mathrm{res}} - \hbar^2 k_1^2 \sin^2(\theta)}}, \tag{8}$$

$$\Im\Sigma^{e-ph,+} = \frac{\alpha\pi m^*\hbar c\Omega^2_{pl}}{\omega_{LO}} \int_0^{2\pi} \frac{d\theta I_{e-ph}\,\Theta(E^+_{\mathrm{res}})}{\sqrt{2m^*E^+_{\mathrm{res}} - \hbar^2 k_1^2 \sin^2(\theta)}}, \tag{9}$$

$$\Im\Sigma^{ee} = \frac{\alpha\pi m^* \hbar c \Omega_{pl}^2}{\epsilon_\infty \omega_{LO}} \int_0^{2\pi} \frac{d\theta I_{ee}\, \Theta(E_{\text{res}})}{\sqrt{2m^* E_{\text{res}} - \hbar^2 k_1^2 \sin^2(\theta)}} \tag{10}$$

(in this regime, also the occupation factors $(1 + n_B - n_F)$ in the three integrands can be safely removed). It can be noticed that the prefactors of Eqs. (9) and (10) have become very similar and proportional to Ω_{pl}^2, and the frequency Ω_{pl}, in turn, is proportional to $\sqrt{\alpha N}$.[29,34] Within the approximations of the present work, all this may justify the similar behavior of τ_{ee} and τ_{e-ph}^{+} with N, but the uncertainty about the overlap integrals I_{ee} and I_{e-ph} is large enough to recommend not to speculate too much in depth about their numerical closeness. Literature simulation results[46] indicate that the scenario may be more complicated: the conduction band edges of the left and right barriers of a blue-emitting InGaN QW may be separated by several hundred meVs by the effect of polarization charges, raising the capture probability by an increase in electron dwell time above the QW. Not only the polarization charges but also the incident electron kinetic energy E_k is an important parameter. Ref. 46 shows that the electron dwell time may vary by orders of magnitude with the value of polarization charges and E_k, thus a more complete transport theory (probably NEGF-based) is needed to include and describe the effects of these two parameters, although maybe preventing to obtain simple expressions for τ as in the present work.

As a final note, in the same low-density regime, from the expression of Ω_{pl}, it follows that both $\Im\Sigma^{ee}$ and $\Im\Sigma^{e-ph,+}$ become proportional to $\alpha^2 N$: since α appears raised to the power of 2, the present formulation is equivalent to the second-order Born approximation[24] when N is low enough, but it provides a better description in the case of arbitrary N.

IV. CONCLUSIONS

We have derived and validated a compact set of expressions for capture time taking into account *ee* and *e-ph* scattering. As suggested by Fig. 2, the authors of Ref. 9 are probably correct when attributing *ee* scattering to the relatively slow capture time governed by carrier population reported in the set B data. The inclusion of a realistic description of *ee* scattering in carrier capture models suitable for device-level simulation (see, e.g., the modeling framework described in Ref. 47) could be, therefore, crucial for LED IQE droop investigations, where high current injection regimes are considered.

In the low carrier density regime, we confirm that considering *e-ph* and *ee* processes, the emission of phonons of frequency ω_- (very close to ω_{LO}) is the most effective capture mechanism. Another important remark is that the slowest elementary processes over the carrier density range considered in set B are *ee* scattering and the emission of phonon-plasmon ω_+ modes: both contribute to a comparable extent, and they remain distinct quantum processes (but not independent, as discussed in Sec. II) with distinct probabilities.

ACKNOWLEDGMENTS

This work was supported in part by the U.S. Army Research Laboratory through the Collaborative Research Alliance (CRA) for MultiScale multidisciplinary Modeling of Electronic materials (MSME).

[1] J. Piprek, Phys. Status Solidi A **207**, 2217 (2010).
[2] G. Verzellesi, D. Saguatti, M. Meneghini, F. Bertazzi, M. Goano, G. Meneghesso, and E. Zanoni, J. Appl. Phys. **114**, 071101 (2013).
[3] V. Avrutin, S. A. Hafiz, F. Zhang, Ü. Özgür, E. Bellotti, F. Bertazzi, M. Goano, A. Matulionis, A. T. Roberts, H. O. Everitt, and H. Morkoç, Turk. J. Phys. **38**, 269 (2014).
[4] C. Weisbuch, M. Piccardo, L. Martinelli, J. Iveland, J. Peretti, and J. S. Speck, Phys. Status Solidi A **212**, 899 (2015).
[5] C. De Santi, M. Meneghini, M. La Grassa, B. Galler, R. Zeisel, M. Goano, S. Dominici, M. Mandurrino, F. Bertazzi, D. Robidas, G. Meneghesso, and E. Zanoni, J. Appl. Phys. **119**, 094501 (2016).
[6] M. Calciati, M. Goano, F. Bertazzi, M. Vallone, X. Zhou, G. Ghione, M. Meneghini, G. Meneghesso, E. Zanoni, E. Bellotti, G. Verzellesi, D. Zhu, and C. Humphreys, AIP Adv. **4**, 067118 (2014).
[7] M. Mandurrino, G. Verzellesi, M. Goano, M. Vallone, F. Bertazzi, G. Ghione, M. Meneghini, G. Meneghesso, and E. Zanoni, Phys. Status Solidi A **212**, 947 (2015).
[8] M. Goano, F. Bertazzi, X. Zhou, M. Mandurrino, S. Dominici, M. Vallone, G. Ghione, F. Dolcini, F. Rossi, G. Verzellesi, M. Meneghini, E. Zanoni, and E. Bellotti, Proc. SPIE **9742**, 974202 (2016).
[9] A. David, C. A. Hurni, N. G. Young, and M. D. Craven, Appl. Phys. Lett. **109**, 033504 (2016).
[10] K. Kálna and M. Moško, Phys. Rev. B **54**, 17730 (1996).
[11] D. S. Sizov, R. Bhat, A. Zakharian, K. Song, D. E. Allen, S. Coleman, and C. en Zah, IEEE J. Sel. Top. Quantum Electron. **17**, 1390 (2011).
[12] W. H. Fan, S. M. Olaizola, J.-P. R. Wells, A. M. Fox, T. Wang, P. J. Parbrook, D. J. Mowbray, and M. S. Skolnick, Appl. Phys. Lett. **84**, 3052 (2004).
[13] W. H. Fan, S. M. Olaizola, J.-P. R. Wells, A. M. Fox, T. Wang, P. J. Parbrook, D. J. Mowbray, and M. S. Skolnick, Appl. Phys. Lett. **91**, 099901 (2007).
[14] M. Takeshima, Jpn. J. Appl. Phys., Part 1 **22**, 491 (1983).
[15] W. Bardyszewski and D. Yevick, J. Appl. Phys. **58**, 2713 (1985).
[16] E. Kioupakis, P. Rinke, K. T. Delaney, and C. G. Van de Walle, Appl. Phys. Lett. **98**, 161107 (2011).
[17] F. Bertazzi, M. Goano, and E. Bellotti, Appl. Phys. Lett. **101**, 011111 (2012).
[18] F. Bertazzi, X. Zhou, M. Goano, G. Ghione, and E. Bellotti, Appl. Phys. Lett. **103**, 081106 (2013).
[19] M. Vallone, F. Bertazzi, M. Goano, and G. Ghione, Phys. Status Solidi B **252**, 971 (2015).
[20] X. Zhang, D. H. Rich, J. T. Kobayashi, N. P. Kobayashi, and P. D. Dapkus, Appl. Phys. Lett. **73**, 1430 (1998).
[21] U. Özgür, M. J. Bergmann, H. C. Casey, Jr., H. O. Everitt, A. C. Abare, S. Keller, and S. P. DenBaars, Appl. Phys. Lett. **77**, 109 (2000).
[22] U. Özgür and H. O. Everitt, Phys. Rev. B **67**, 155308 (2003).
[23] H.-C. Wang, Y.-C. Lu, C.-Y. Chen, and C. C. Yang, Appl. Phys. Lett. **89**, 011906 (2006).
[24] S. M. Goodnick and P. Lugli, Phys. Rev. B **37**, 2578 (1988).
[25] P. Sotirelis, P. von Allmen, and K. Hess, Phys. Rev. B **47**, 12744 (1993).
[26] P. Sotirelis and K. Hess, Phys. Rev. B **49**, 7543 (1994).
[27] S.-C. Lee and I. Galbraith, Phys. Rev. B **59**, 15796 (1999).
[28] H. Haug and S. W. Koch, Phys. Rev. A **39**, 1887 (1989).
[29] G. D. Mahan, *Many-Particle Physics*, 2nd ed. (Plenum Press, New York, 1990).
[30] A. L. Fetter and J. D. Walecka, *Quantum Theory of Many-Particle Physics*, 3rd ed. (Dover Publications, New York, 2003).
[31] S. Chiaria, E. Furno, M. Goano, and E. Bellotti, IEEE Trans. Electron Devices **57**, 60 (2010).
[32] I.-H. Tan, G. L. Snider, L. D. Chang, and E. L. Hu, J. Appl. Phys. **68**, 4071 (1990).
[33] J. Wang, K. W. Kim, and M. A. Littlejohn, Appl. Phys. Lett. **71**, 820 (1997).
[34] H. Haug and S. W. Koch, *Quantum Theory of the Optical and Electronic Properties of Semiconductors* (World Scientific Publishing, Singapore, 2004).

[35]S. A. Levetas and M. J. Godfrey, Phys. Rev. B **59**, 10202 (1999).
[36]M. Vallone, J. Appl. Phys. **91**, 9848 (2002).
[37]H. Haug and A.-P. Jauho, *Quantum Kinetics in Transport and Optics of Semiconductors*, 2nd ed. (Springer, Berlin, 2008).
[38]L. Bányai, Q. T. Vu, B. Mieck, and H. Haug, Phys. Rev. Lett. **81**, 882 (1998).
[39]L. P. Kadanoff and G. Baym, *Quantum Statistical Mechanics. Green's Function Methods in Equilibrium and Nonequilibrium Problems* (W. A. Benjamin, New York, 1962).
[40]S. Karpov, Opt. Quantum Electron. **47**, 1293 (2015).
[41]J. Piprek, F. Römer, and B. Witzigmann, Appl. Phys. Lett. **106**, 101101 (2015).
[42]B. Romero, J. Arias, I. Esquivias, and M. Cada, Appl. Phys. Lett. **76**, 1504 (2000).
[43]S.-B. Choi, J.-P. Shim, D.-M. Kim, H.-I. Jeong, Y.-D. Jho, Y.-H. Song, and D.-S. Lee, Appl. Phys. Lett. **103**, 033901 (2013).
[44]The differences between the plots of $\tau^{\pm}_{e-ph}(N)$ reported in Fig. 2 and in our previous work[19] derive from the use of erroneous values of the QW/barrier thickness[13] reported in Ref. 12.
[45]D. Saguatti, L. Bidinelli, G. Verzellesi, M. Meneghini, G. Meneghesso, E. Zanoni, R. Butendeich, and B. Hahn, IEEE Trans. Electron Devices **59**, 1402 (2012).
[46]M. F. Schubert and E. F. Schubert, Appl. Phys. Lett. **96**, 131102 (2010).
[47]M. Grupen and K. Hess, IEEE J. Quantum Electron. **34**, 120 (1998).